




The role of Sn trace addition in the precipitation behavior and strengthening of the wrought Al–Cu–Mn-based alloy

T. K. Akopyan^{1*} , N. V. Letyagin¹, N. A. Belov¹, A. S. Fortuna¹, and X. D. Nguen¹

¹National University of Science and Technology MISiS, 4 Leninsky pr., Moscow, Russia 119049

Received: 9 April 2023

Accepted: 18 April 2023

Published online:

3 May 2023

© The Author(s), under exclusive licence to Springer Science+Business Media, LLC, part of Springer Nature 2023

ABSTRACT

The enhancing effect of low melting trace additions (Sn, Cd, In) on the precipitation hardening in the Al–Cu based alloys accounts for the great practical importance of this phenomenon. However, to date, the influence of Sn micro-addition, either separately or jointly with other ones, on the precipitation structure and hardening of the wrought 2219-type alloys based on the Al–Cu–Mn system remains unexplored. In this study, the effect of 0.1 wt% (0.02 at.%) Sn trace addition on the structure and mechanical properties of the new Al–4Cu–1.5Mn (wt%) alloy has been studied using computational (thermodynamic calculations) and experimental techniques. Analysis of microhardness has revealed that the peak hardness at aging of the wrought model Sn-containing alloy reaches ~ 120 HV which is about 43% higher than for the Sn-free alloy. Transmission electron microscopy analysis of the peak-aged hot-rolled sheet alloys has revealed that trace addition dramatically changes the precipitation structure leading to the formation of much finer precipitates (with an average length of 55–60 nm) with a higher number density. Uniaxial tensile tests of the wrought and peak-aged samples have revealed that the mechanical properties of the model Al₄Cu_{1.5}Mn_{0.1}Sn alloy (UTS ~ 402 MPa, YS ~ 323 MPa and elongation ~ 9.7%) are very close to those of the industrial 2219-type alloy. However, the new alloy contains a much lower concentration of copper and a superior fraction of Al₂₀Cu₂Mn₃ phase dispersoids the influence of which on the mechanical properties should be further studied in detail.

Handling Editor: Sophie Primig.

Address correspondence to E-mail: nemiroffandtor@yandex.ru

Introduction

Wrought Al–Cu–Mn alloys (2xxx family) are still most widely used in industry due to their strength to weight ratio and heat resistance [1]. However, these alloys require continuous improvement because of the growing demand for light weight and high manufacturability with a short production cycle [2]. A brilliant example is the model Al₂Cu₂Mn alloy showing potential to become the basis for the design of new generation heat-resistant alloys as a sustainable alternative to the 2219 alloys [3]. The latter possibility is due to the higher heat resistance of the new alloy (the YS after annealing at 400 °C is 210 MPa compared to 86 MPa for the 2219 alloy) combined with a significantly lower content of copper and a far shorter technological route due to the exclusion of homogenization annealing. The higher heat resistance of the new alloy is caused by the formation of a far greater fraction of T-phase (Al₂₀-Cu₂Mn₃) dispersoids.

On the other hand, the strength of the 2219-type alloys is determined by precipitation hardening caused by the formation of metastable precipitates of the θ' (Al₂Cu) phase [4–6]. Precipitation hardening is an important mechanism of strength improvement in aluminum alloys which is mainly determined by the number density, crystal structure and size of precipitates [7]. Accordingly, greatest attention is paid to various combinations of aging protocols as well as introduction of various additives improving the age hardening response of the AA2219-type alloys. For example, the AA2519 alloy with a minor Mg addition and a reduced Cu content was developed as a new grade of the AA2219 alloy [8]. The Cu–Mg–vacancy complexes form effective nucleation sites for GP zones thus increasing their nucleation rate. Further the GP zones transform in situ to the θ'' -phase and Mg favors the precipitation of the θ'' -phase [4] with an increased number density. Another direction of the studies is focused on controlling the precipitation hardening response throughout microalloying with low melting or precious metals including Sn [9–14], In [15–18], Cd [19, 20], Pb [21], Ag [22–26] and Au [27, 28]. Al–Cu alloys with any of these trace additions reach a much higher peak hardness due to the formation of much finer precipitates of the θ' -phase (or in some cases the Ω -phase [23, 25, 26]) with a high number density. Moreover, it is safe to say that tin is

of scientific and industrial interest among the above-mentioned additions due to its high availability, presence in secondary raw materials and a strong effect at extremely low concentrations. Sn trace addition in Al–Cu alloys dramatically suppresses clustering at quenching and natural aging because of strong interaction between vacancies and trace element atoms [29–32]. In turn, this interaction leads to an accelerated decomposition of the aluminum solid solution (Al) coupled with the formation of precipitates at artificial aging. Indeed [11], upon aging at 175 °C, the peak hardness of the Al_{3.5}Cu_{0.1}Sn alloy is about 20% higher than that of the Sn-free alloy and is achieved in a shorter aging time (2 h vs. ~ 12 h). Transmission electron microscopy and 3D atom probe tomography revealed that the increased hardness of the ternary alloy is due to the formation of fine plate-like θ' -phase precipitates which are at least two times smaller and have at least a twice as high number density as compared to those in the Sn-free alloy. Finally, Sn-containing Al–Cu alloys show a simultaneous increase in the strength and fracture toughness [33]. Thus, the effect of Sn trace addition on precipitation hardening accounts for its great importance for industry.

One should note that systematic studies of the effect of Sn trace addition on the precipitation hardening have been carried out mainly for ternary Al–Cu–Sn model alloys [11, 12, 16, 21, 33]. Some studies have also dealt with the effect of Sn trace additions on the properties of the copper-containing alloys based on other systems such as Al–Si–Cu [9, 10], Al–Cu–Mg [13, 29] and Al–Cu–Mn [17]. In the latter work, the effect of some micro-additions (Zr, Sc, Sn, In) on the precipitation structure and hardening was studied for the cast alloy based on Al–4.6%Cu–0.4%Mn–0.2%Ti. And although the work reported a significant increase in the mechanical properties of the alloy, the influence of Sn micro-addition, either separately or jointly with other ones, on the precipitation structure and hardening of the wrought 2219-type alloys based on the Al–Cu–Mn system remains unexplored.

One should note that the content of Mn in the 2219 alloy is limited by 0.5%. A higher content of Mn leads to the formation of a greater fraction of copper-containing T-phase dispersoids which in turn reduce the copper concentration in the aluminum solid solution (Al). The result of this decrease is a smaller number of the θ' -phase precipitates at aging and therefore less hardening achieved. However, due to the aging-

enhancing effect of tin trace addition, the concentration of Mn in the 2219-type alloys can be substantially increased. Moreover, to achieve the same strength as for the classical 2219 alloy, much lower concentration of copper is needed in the Sn-containing alloy.

Based on the above, the main purpose of this work was to analyze the effect of Sn trace addition on the phase composition, precipitation structure and mechanical properties of the new Al–Cu–Mn-based model alloy with a higher Mn content and a lower Cu concentration compared to that for the industrial 2219-type alloys. One should note that the industrial 2219 alloy contains, along with manganese, other micro-additions such as zirconium, vanadium and titanium, as well as common impurities such as silicon and iron the influence of which on the properties of the Sn-containing alloys should be further studied in detail in order to recommend new materials for industrial applications.

Materials and methods

The main subjects of the study were 2 alloys (hereinafter Al4Cu1.5Mn and Al4Cu1.5Mn0.1Sn) the chemical composition of which according to spectral analysis (Oxford Instruments) is presented in Table 1 from which it can be seen that the actual compositions are quite close to the target one. The melting was carried out in a GRAFICARBO resistance furnace in a graphite crucible from high purity aluminum 1199 (99.99 wt% Al). Cu and Sn were introduced into the aluminum melt in the form of pure metals (99.9 wt% Cu and 99.9 wt% Sn) and Mn in the form of a Al–10 wt% Mn master alloy. After melting of the basic components, the melt was held for 5–10 min to provide its homogenization and to remove the slag, and then the metal was cast into a graphite mold with a working cavity of 10 × 40 × 180 mm in size at 780–800 °C.

The obtained cast specimens were subjected to homogenization annealing at 450 or 510 °C for 10 h followed by water quenching at room temperature

(~ 23 °C). Some specimens after annealing at 510 °C were further treated by hot rolling at 400 °C with an 80% reduction. The obtained 2 mm sheet samples were solid solution heat-treated at 510 °C for 1 h followed by water quenching at room temperature. Both as-quenched cast and as-quenched wrought specimens were subjected to 175 °C aging for different holding time. The heat treatment was performed in muffle electric furnaces in an air atmosphere with a temperature accuracy of ~ 3 K.

The microstructure was examined using transmission electron microscopy (TEM, Jeol JEM 1400 microscope) and scanning electron microscopy (SEM, TESCAN VEGA 3) with an energy-dispersive X-ray spectroscopy analysis system (EDS, OXFORD Aztec, Oxford Instruments, Oxfordshire, UK) and Aztec software. Polished samples were used for the studies. The metallographic samples were ground with SiC abrasive paper and polished with 1 µm diamond suspension. 1% hydrogen fluoride (HF) water solution was used for etching. Thin foils for TEM were prepared by two-jet electrolytic polishing on a STRUERS Tenupol-5 installation at a 21 V voltage. A solution of nitric acid in methanol in a ratio of 1:4 (vol.) cooled to – 15 °C was used as an electrolyte.

The as-quenched samples were subjected to artificial aging at 175 °C (448 K) for studying the influence of aging time on the hardness and specific electrical conductivity. The Vickers hardness (Hv) was measured using a DUROLINE MH-6 setup (METKON Instruments) with a load of 1 kg and a dwell time of 10 s. At least five measurements were performed for each sample. The specific electrical conductivity (EC) of the samples was determined using the eddy current method with a VE-26NP eddy structurescope.

Room-temperature tensile tests were conducted for the peak-aged hot-rolled 2 mm sheets on a universal testing machine, model Zwick Z250 (the velocity of loading was 10 mm/min). The flat rectangular test samples without grippers having a length of 110 mm and a width of 10 mm were made from the 2 mm hot-rolled sheets. The fracture surfaces of the tensile test specimens were analyzed after the tests.

Table 1 Target and actual chemical composition of experimental alloys

Alloy	Target/actual concentration, wt%				
	Al	Cu	Mn	Fe	Sn
Al4Cu1.5Mn	Balance	4.0/4.11	1.5/1.35	0/0.04	0/–
Al4Cu1.5Mn0.1Sn	Balance	4.0/4.14	1.5/1.40	0/0.09	0.1/0.12

Theoretical assessment of the phase equilibria in the Al–Cu–Mn system as well as quantitative analysis of the phase composition of the specified alloys were carried out using the Thermo-Calc software (TCAL4 and TTAL5 databases [34]).

Results

Theoretical assessment of phase composition

Figure 1a shows the vertical isopleth of the ternary Al₄Cu–Mn system at the absolute minimum of the free energy, i.e., in equilibrium. One can see that, according to the calculation, at a manganese concentration of 1.5 wt%, the model Al₄Cu alloy falls into the boundary of the primary solidification field of the aluminum solid solution (Al) and the binary Al₆Mn compound, i.e., the solidification of the alloy should start with the formation of the binary eutectic (Al) + Al₆Mn phase. Equilibrium solidification continues with the peritectic reaction $L + Al_6Mn \rightarrow Al_{20}Cu_2Mn + (Al)$ leading to the formation of the ternary Al₂₀Cu₂Mn compound. The solidification ends in the binary phase field Al₂₀Cu₂Mn + (Al). However, it is well known [35] that during solidification up to 2 wt% manganese can dissolve in (Al) since a metastable solidification sequence takes place under actual conditions. Due to the latter fact, the equilibrium vertical isopleth was recalculated for metastable conditions developed upon the addition of Sn (Fig. 1b). For obtaining a metastable equilibrium, the calculation program was set such that all manganese is dissolved in aluminum and thus no Mn-containing phases can form. One can see that in this case the quaternary Al₄Cu_{1.5}Mn–Sn system transforms to the ternary Al–Cu–Sn one like earlier reported [11]. All Mn is dissolved in the aluminum solid solution. One can also see that the solubility limit of tin in (Al) is close to that obtained for the equilibrium state and is about 0.5 wt% (or ~ 0.1 at.%) at 500 °C. For the alloys containing up to 0.5 wt% Sn, one can expect the reappearance of the tin-saturated liquid phase after solidification. The solidification ends at 230 °C which is slightly below the melting point of Sn. One should note that the obtained calculated data on the solubility limit of tin in (Al) are obviously overestimated. Indeed, according to our previous study [10], the solubility of Sn in

(Al) in the ternary Al–Si–Cu system is about 0.02 ± 0.01 at.% which is in a good agreement with earlier data [36], indicating that the solubility limit of tin in (Al) in the binary Al–Sn system is 0.026 at.% or 0.11 wt%.

After the solidification, the aluminum solid solution proves to be supersaturated with manganese, and further high-temperature annealing should lead to (Al) decomposition with the formation of Mn-containing dispersoids. Figure 1c, d shows two isothermal sections of the Al–Cu–Mn system for 450 and 510 °C. The lower temperature is the maximum one recommended for obtaining relatively fine dispersoids of the Mn-containing phases, while the higher temperature ensures the complete dissolution of copper in aluminum. Indeed, as can be seen from Fig. 1c, the Al₄Cu_{1.5}Mn alloy (indicated by a circle) is in the ternary (Al) + T(Al₂₀Cu₂Mn₃) + Al₂Cu phase field at 450 °C. The binary phase field (Al) + T(Al₂₀Cu₂Mn₃) at this temperature is quite narrow, and the concentration of copper must be further reduced to 2.5–3.0% in order for the alloy to fall into this region. At the higher temperature (510 °C), the complete dissolution of Al₂Cu in (Al) can be expected (this is also well confirmed by the Al–Cu binary diagram [37]). The binary phase field (Al) + T(Al₂₀Cu₂Mn₃) broadens significantly, and the alloy falls within it. Although the higher temperature ensures the complete dissolution of Cu in the aluminum matrix, which in turn should lead to a higher precipitation response, this will also lead to coarsening of the dispersoids thus reducing their influence.

Other calculated data obtained using Thermo-Calc (Table 2) allow one to quantitatively assess the chemical composition of the aluminum solid solution (Al), and the fraction of the Al₂₀Cu₂Mn₃ and Al₂Cu phases in equilibrium with (Al) depends on the alloys composition and annealing temperature. Analysis was performed for two different contents of Mn, i.e., 0.2 and 1.5 wt% and Cu, i.e., 4 and 6 wt% at 450 and 540 °C. The lower temperature corresponds to the upper recommended annealing temperature limit for the formation of relatively fine Al₂₀Cu₂Mn phase dispersoids, while the higher temperature is the one used for solid solution treatment of the 2219-type alloys. One can see that the amount of the Al₂₀Cu₂Mn₃ phase is determined by the content of manganese in the alloy and depends but slightly on temperature. Indeed, for both contents of copper, the

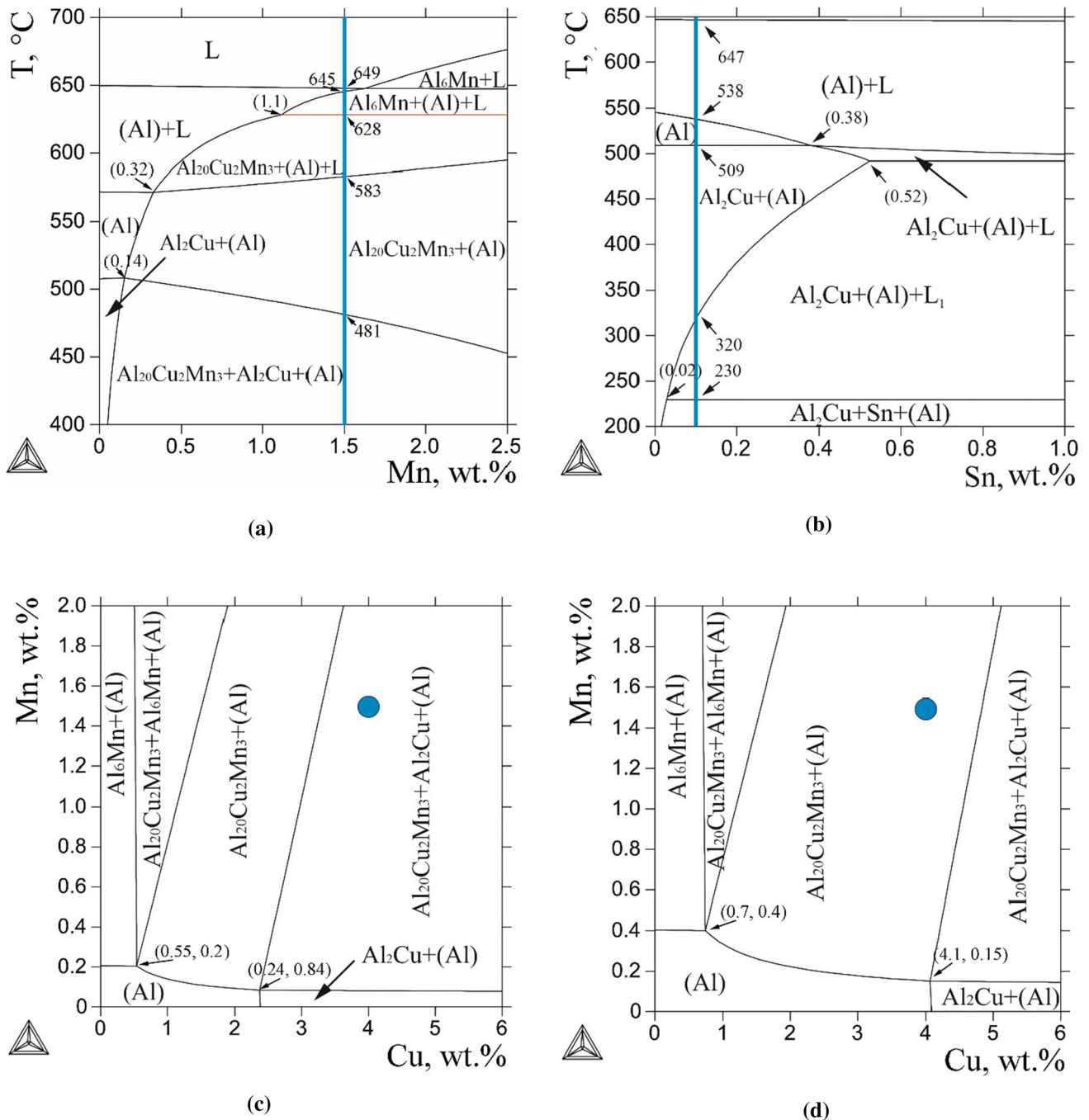


Figure 1 **a** Equilibrium vertical isopleth of the Al-4Cu-Mn system; **b** metastable vertical isopleth of the Al-4Cu-1.5Mn-Sn system. The vertical lines correspond to the composition of the alloys: **a** Al4Cu1.5Mn and **b** Al4Cu1.5Mn0.1Sn. The main phase transformation temperatures for the alloys are indicated by arrows

along the vertical lines and the compositions (wt%) of some points on the diagram are indicated in brackets. Equilibrium isothermal sections of the Al-Cu-Mn system at **c** 450 °C and **d** 510 °C. The chemical composition of the Al4Cu1.5Mn alloy is indicated by the circle.

fraction of the Al₂₀Cu₂Mn₃ phase varies from 0.6 to 7.2% at 450 °C and from 0.04 to 6.65% at 540 °C with the Mn content varying from 0.2 to 1.5 wt%. However, the content of copper in the alloys determines

the content of the residual fraction of the Al₂Cu phase and the composition of the (Al) solid solution. For example, in the alloy containing 6.0% Cu at 450 °C the residual fraction of the Al₂Cu phase varies from

Table 2 Calculated composition of aluminum solid solution (Al) and weight fractions of phases in equilibrium with (Al) as a function of annealing temperature and Al–Cu–Mn alloys composition

Concentration of elements in Al–Cu–Mn alloys, wt%		Annealing temperature, °C	Composition of (Al), wt%		Fractions of phases in equilibrium with (Al), wt%	
Cu	Mn		Cu	Mn	Al ₂₀ Cu ₂ Mn ₃	Al ₂ Cu
6	0.2	450	2.4	0.08	0.6	7.0
		510	4.1	0.15	0.28	4.0
		540	5.3	0.19	0.04	1.5
	1.5	450	2.4	0.08	7.2	5.3
		510	4.1	0.15	6.9	2.4
		540	5.3	0.19	6.65	0.7
4	0.2	450	2.4	0.08	0.6	3.1
		510	4.0	0.15	0.24	–
	1.5	450	2.4	0.08	7.2	1.4
		510	3.2	0.17	6.75	–

7.0 to 5.3% with the Mn content varying from 0.2 to 1.5 wt%, while an increase in temperature to 540 °C reduces this amount to 1.5 wt% at 0.2 wt% Mn and to 0.7 wt% at 1.5 wt% Mn. An increase in the Mn content leads to a decrease in the content of the residual fraction of the Al₂Cu phase due to the formation of the Al₂₀Cu₂Mn phase. A decrease in the content of copper in the alloy to 4% leads to a substantial decrease in the content of the residual fraction of the Al₂Cu phase. For instance, the residual fraction of the Al₂Cu phase is 3.1% at 450 °C for a Mn content of 0.2% and it decreases to 1.4% for a Mn content of 1.5%. At above 510 °C, copper dissolves completely in aluminum regardless of the manganese content in the alloys containing 4% Cu.

The actual composition of the aluminum solid solution varies significantly depending on the temperature and manganese content. One should note that the actual composition of (Al) after solid solution treatment mainly determines the precipitation hardness response at aging. For the 2219-type alloys (based on Al–6 wt% Cu–0.2 wt% Mn), due to the excess of copper, the actual composition of (Al) is determined by the temperature, and an increase in the manganese content to 1.5% does not affect it (Table 2). At the solid solution treatment temperature (540 °C), the concentration of Cu in (Al) reaches about 5.3% which is close to the solubility limit of copper in aluminum. A decrease in the copper content to 4% makes the actual composition of (Al) quite sensitive to the manganese content. Indeed, as can be seen from Table 2, the solubility of copper in (Al) at the lower temperature (450 °C) is same for all the

alloys while an increase in temperature to 510 °C reveals some differences depending on the Mn content. At the lowest Mn content of 0.2%, one can see that almost all copper contained in the alloy (~ 4%) is dissolved in (Al), while at 1.5% Mn, the copper solubility drops to ~ 3.2%.

Finally, the composition of (Al) after solid solution treatment determines the fraction of the strengthening metastable θ' phase. The expected fraction of the metastable θ' phase at the aging temperature was also calculated using the Thermo-Calc program. For obtaining a metastable equilibrium, the formation of the metastable θ' phase (which is included in the thermodynamic TCAL4 database used) instead of the stable θ phase was set in the program. Figure 2 shows the expected fraction of the stable Al₂Cu(θ) and metastable θ' phases at the possible aging temperature of 175 °C for different compositions of the aluminum solid solution. One can see that the fraction of the metastable phase is always lower at the same copper content. For the 2219-type alloy after high-temperature solid solution treatment followed by aging at 175 °C, the formation of about 9% metastable θ' phase can be expected. For the model Al4Cu1.5Mn alloy studied in the work, one can expect the formation of 3.7 to 5.2% metastable phase (depending on the actual composition of (Al)) which is much lower than that for the industrial alloy. In contrast, the fraction of Al₂₀Cu₂Mn phase dispersoids in the new alloy containing 1.5 wt% Mn is much higher (see Table 2) compared with the base 2219 alloy composition (Al–6 wt% Cu–0.2 wt% Mn).

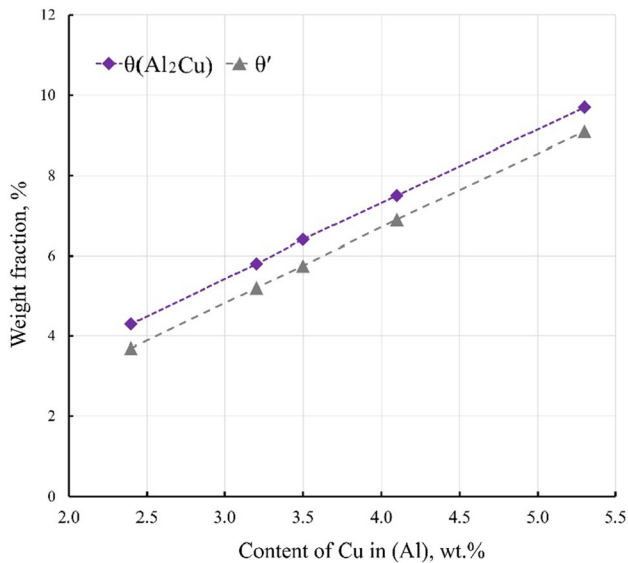


Figure 2 Calculated weight fraction of stable θ (Al₂Cu) and metastable θ' phases at 175 °C depending on (Al) composition.

Analysis of microstructure of as-cast and homogenized alloys

The main structure constituent of both the Al4Cu1.5Mn and Al4Cu1.5Mn0.1Sn as-cast alloys are eutectic colonies formed by the copper-containing phase. The eutectic colonies have a network morphology or a strip shape with a network structure (Fig. 3a, b). According to EDS analysis, the eutectic phase observed in both the as-cast alloys is confirmed to be the θ (Al₂Cu) phase, mainly consisting of Al and Cu with an Al/Cu molar ratio of approximately 2:1. Most Cu is segregated in the eutectic phase, while its concentration in (Al) is about 1.1 wt%. Most manganese is dissolved in the aluminum matrix. However, some areas that correspond to the rare inclusions of the Mn-containing compound are also revealed (Fig. 3c). At a higher magnification, the Al4Cu1.5Mn0.1Sn alloy structure explicitly exhibits Sn inclusions sticking to the θ phase (Fig. 3b, c). The described structure containing a high fraction of brittle non-equilibrium θ (Al₂Cu) phase is not appropriate for deformation, and therefore the experimental alloys require homogenization annealing providing for the dissolution of the non-equilibrium eutectic. Furthermore, the formation of Al₂₀Cu₂Mn₃ dispersoids should also be expected at high-temperature annealing. The influence of annealing was examined for both 450 and 510 °C.

Analysis revealed that undissolved eutectic θ (Al₂Cu) phase inclusions with a morphology largely inherited from the as-cast structure can be still observed in a high amount in both alloys after annealing at 450 °C (Fig. 4a and c). Furthermore, one can observe the intense formation of a high amount of Mn-containing phase dispersoids in fact covering the entire body of the grain. It is interesting to note that in some local places inside the grains of both alloys, there are regions of discontinuous decomposition (DD) where the number density of the dispersoids is much lower and their linear size is much larger (up to several microns). The formation of such regions can be accounted for by the local redistribution of Mn atoms. For instance, the precipitation of dispersoids at the grain boundaries (marked by arrows in Fig. 4b and d) leads to a decrease in the concentration of Mn in the near-boundary region. As a result, one can observe the formation of coarser dispersoids with a lower number density in the near-boundary regions. It seems that this is the case for the structure presented by way of example in Fig. 4b. Another origin of this effect can be associated with the natural distribution of dissolved Mn atoms in (Al) at solidification processes. Nonetheless, an increase in the annealing temperature to 510 °C leads to a much more complete dissolution of the non-equilibrium eutectic phase (Fig. 5a and c). Most of the remaining crystals are insoluble by nature; they consist of Mn and are formed during alloy solidification. The structure of the dispersoids becomes obviously coarser (Fig. 5b) which is especially well detectable in the above-mentioned discontinuous decomposition regions. However, for the Sn-containing alloy the structure of the dispersoids especially in the DD regions (Fig. 5d) seems to be finer than that for the Sn-free alloy.

Structure at deformation and solid solution treatment

At the deformation treatment, the experimental alloys demonstrated high processability expressed as the absence of surface defects and typical edge cracks. The structure of the as-deformed alloys does not differ much. One should note that hot deformation of the model alloys significantly improved the morphology of dispersoids that were found to be plate (average length up to 500 nm) and uniformly distributed (Fig. 6a, b). Some of the dispersoids can

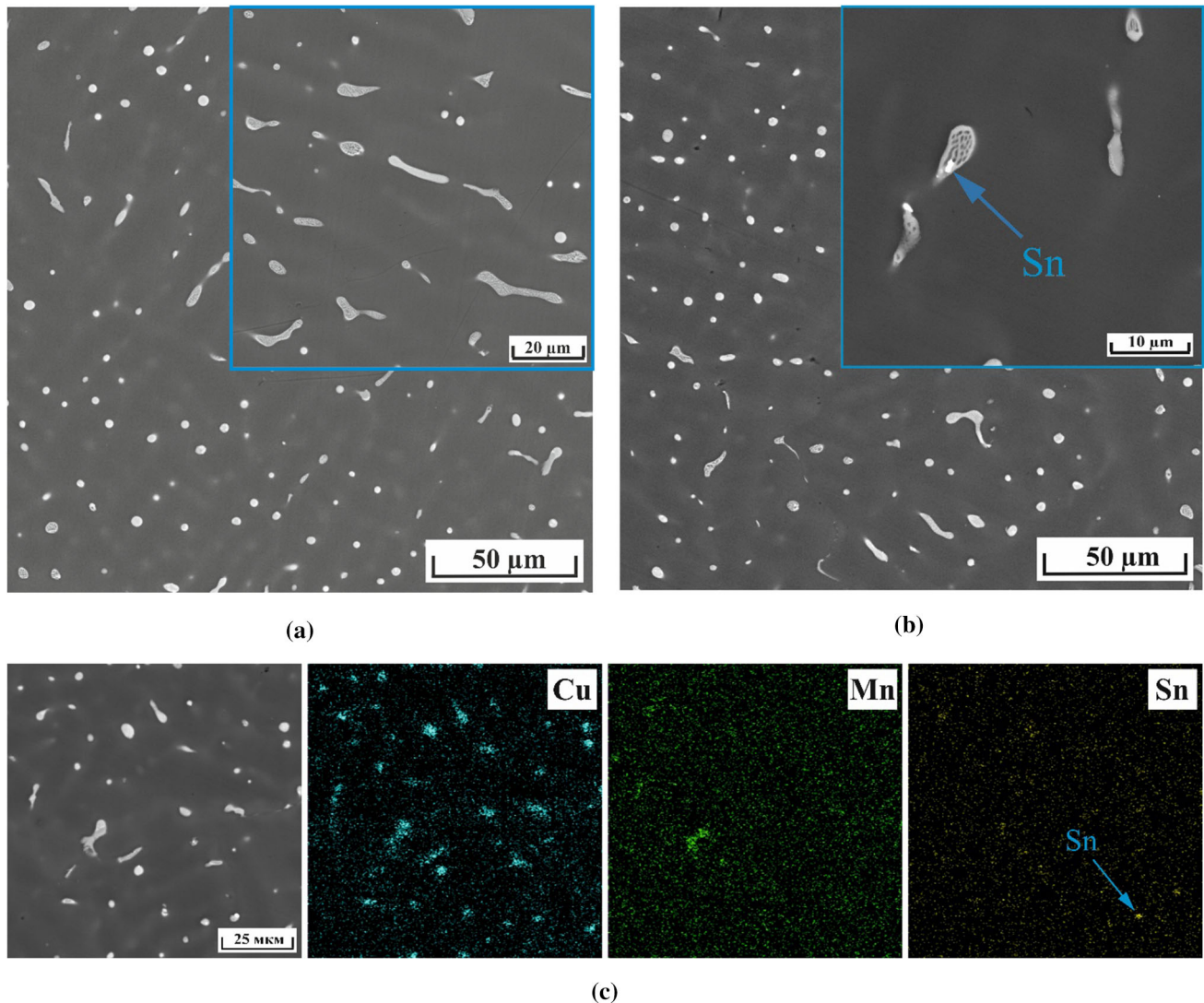


Figure 3 As-cast structures of **a** Al₄Cu_{1.5}Mn and **b** Al₄Cu_{1.5}Mn_{0.1}Sn alloys and **c** elemental mapping obtained from the selected area (leftmost figure) for the Al₄Cu_{1.5}Mn_{0.1}Sn alloy. SEM.

be detected at the grain and sub-grain boundaries confirming their pinning ability (Fig. 6c), and the experimental diffraction patterns are good evidence that the dispersoids belong to the Al₂₀Cu₂Mn₃ phase [38]. In addition, one can also observe the formation of intensely deformed zones with a high number density of dislocations around dispersoids within the grains (Fig. 6d). It is well known [39] that the localization of deformation in such a manner is beneficial for more intense strain hardening.

The structure of the as-quenched alloys does not differ either (Fig. 7a, b). The grain and sub-grain boundaries are not observed anymore, suggesting intense grain growth because of far-reaching recrystallization processes. Inside the grains, one can

observe two types of the local distribution of the Al₂₀Cu₂Mn₃ phase dispersoids. Regions where dispersoids are much finer and their number density is much higher alternate with regions containing much coarser dispersoids with a low number density. However, the regions of the second type are far less; they are inherited from the as-cast structure. In addition, even after solid solution treatment at the higher temperature, one can observe high dislocation density locally retained in the vicinity of the Al₂₀Cu₂Mn₃ phase dispersoids (Fig. 7b). The influence of the structure forming as a result of the deformation and solid solution treatment on the precipitation hardening response was further studied for aging.

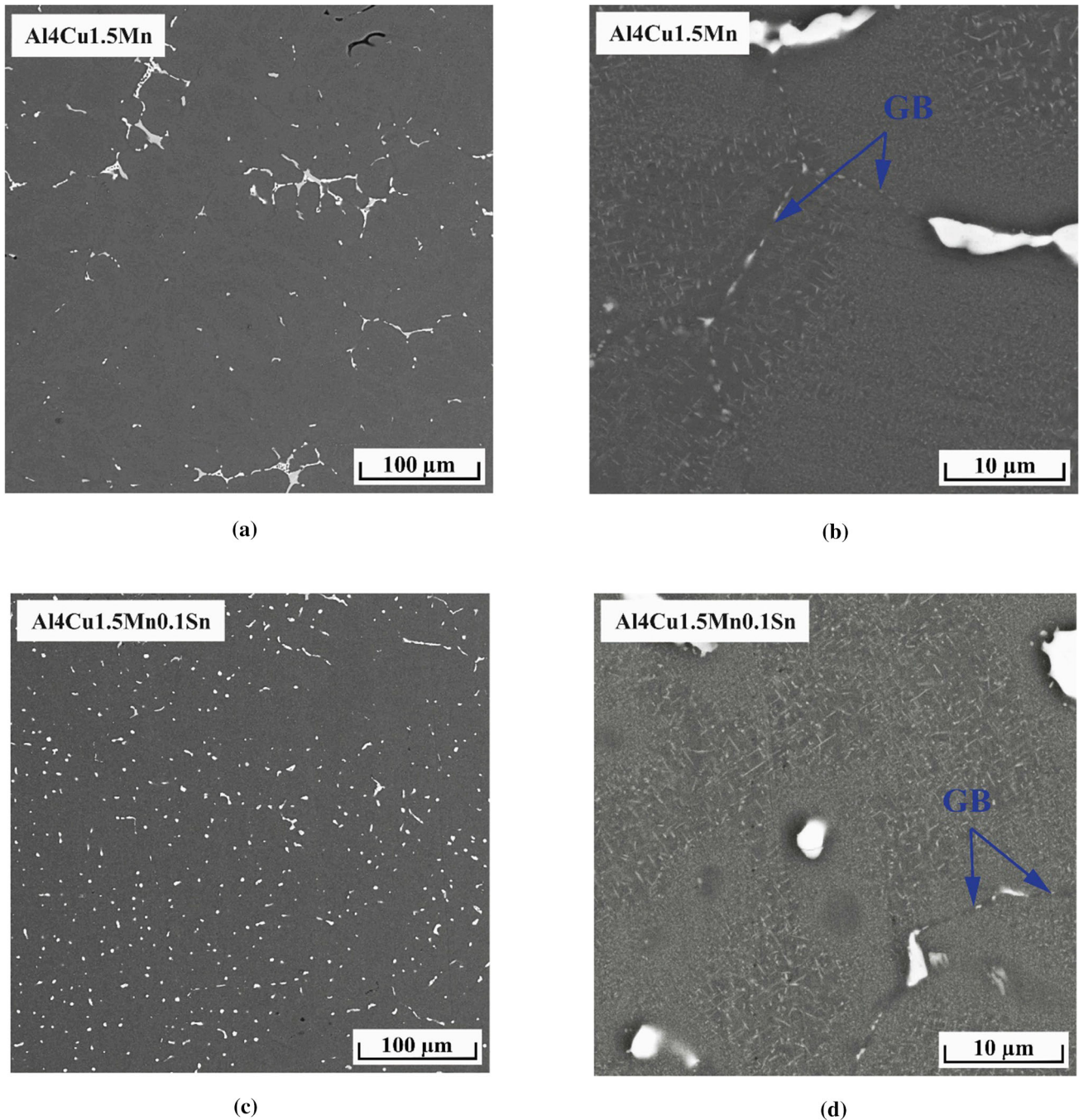


Figure 4 Microstructure of **a, b** Al4Cu1.5Mn and **c, d** Al4Cu1.5Mn0.1Sn alloys after annealing at 450 °C for 10 h. Designation GB denotes grain boundaries.

Hardness and specific electrical conductivity at aging

Two temperatures of solid solution treatment, i.e., 450 and 510 °C, were considered for the castings. Data on the change in the hardness and specific electrical conductivity (EC) during aging at 175 °C for

the castings preliminary heat-treated at 450 °C are presented in Fig. 8. One can observe that annealing followed by quenching leads to some increase in the hardness of the alloys as compared to the as-cast state (~ 66 HV vs. ~ 77 HV, roughly the same for both alloys) while the EC increases substantially (14 vs. 25 MS/m). This result is a consequence of the

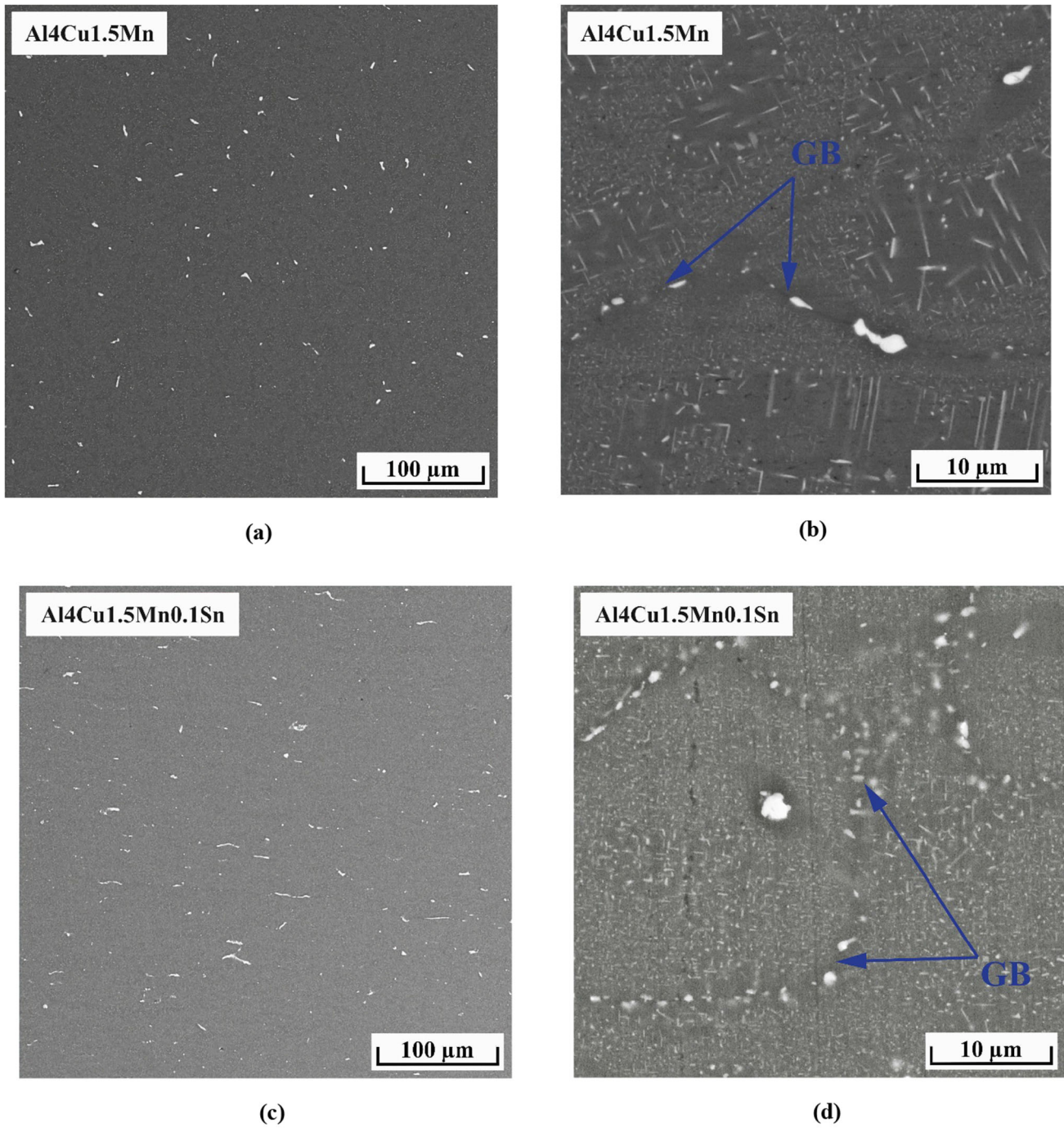


Figure 5 Microstructure of a, b Al4Cu1.5Mn and c, d Al4Cu1.5Mn0.1Sn alloys after annealing at 510 °C for 10 h. Designation GB denotes grain boundaries.

decomposition of the aluminum solid solution (Al) with the formation of the $\text{Al}_{20}\text{Cu}_2\text{Mn}_3$ phase dispersoids in both alloys. Thus, while the influence of high fraction of this type of dispersoids on the hardness is noticeable (the effect on hardness of dissolved copper should also be taken into account), the influence of

the dissolved manganese atoms on the EC is enormous and one of the strongest among other additives in aluminum alloys [40, 41]. Further aging at 175 °C has a very small effect on the hardness of the base Sn-free alloy over the entire experimental exposure time, but after 6 h of aging a moderate increase in the

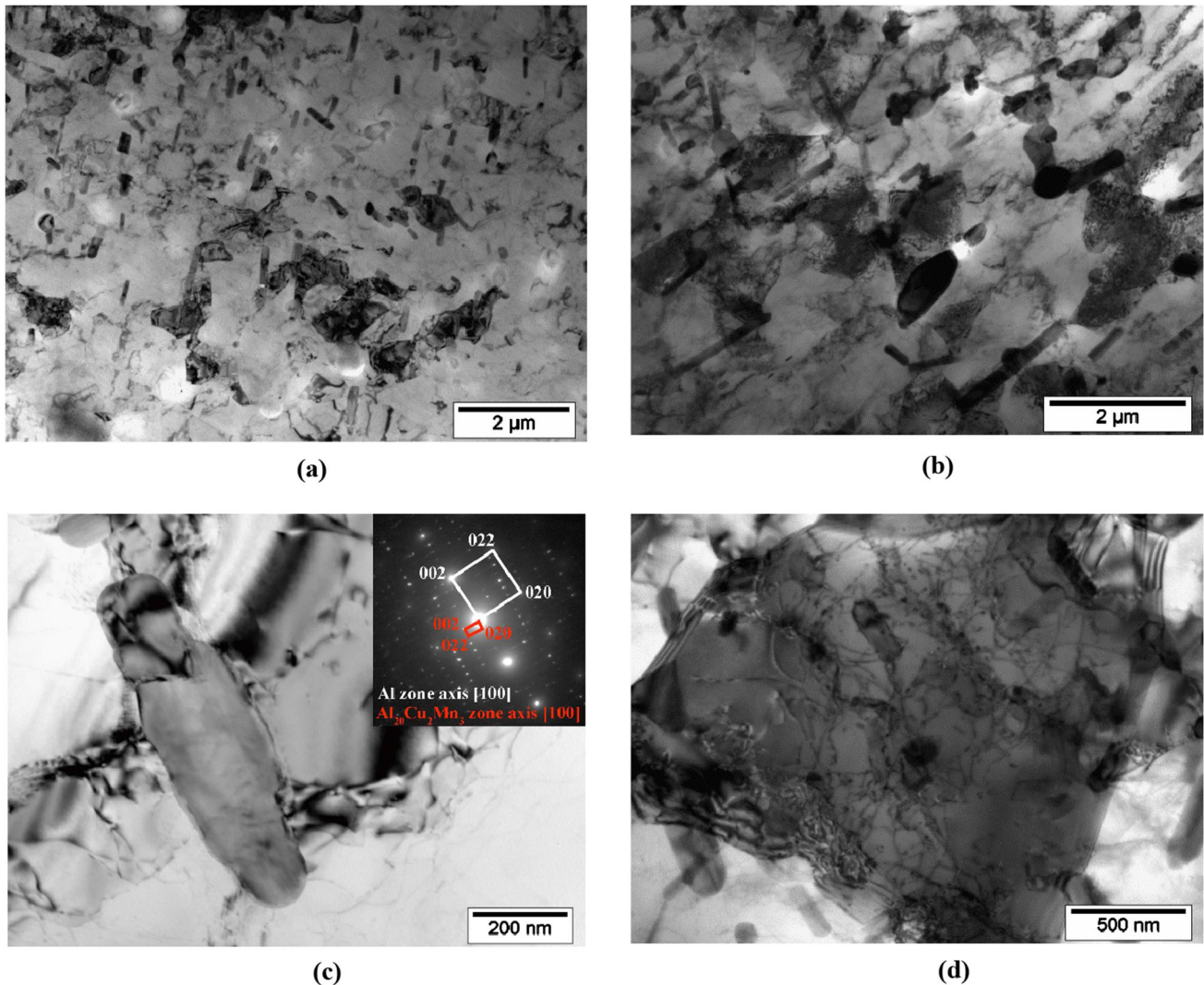


Figure 6 TEM structure of hot-rolled sheet Al₄Cu_{1.5}Mn_{0.1}Sn alloy with a 80% reduction. **a**, **b** general view; **c**, **d** higher-magnification images revealing sub-grains boundaries, location of

Al₂₀Cu₂Mn₃ dispersoids and local dislocation structure and **c** also represents selected area diffraction patterns (SADP) taken along [100] Al zone axis.

hardness can be observed for the Sn-containing alloy. Indeed, during aging one can observe a moderate increase in the hardness by $\sim 13\%$, reaching ~ 85 HV in 15 h. The relatively weak precipitation hardening response observed can be accounted for by insufficient saturation of the aluminum matrix with copper due to an insufficiently high solid solution treatment temperature. One should also note that the EC of the Sn-containing alloy is somewhat higher than that of the Sn-free alloy which is a direct result of the greater decomposition degree of (Al) in the former alloy.

An increase in the solid solution (SS) treatment temperature to 510 °C substantially increases the

precipitation hardening response of the Sn-containing alloy in both the cast and wrought states (Fig. 9a). On the contrary, quenching followed by 175 °C aging of the cast Sn-free alloy affects its hardness but slightly. After deformation and SS heat treatment, the hardness of both the Sn-free and Sn-containing alloys in the as-quenched state turns lower than that for the castings. The data obtained can be accounted for by the minor decomposition of (Al) at SS treatment and quenching. The latter assumption can be confirmed by the slightly higher EC of the deformed alloys in the as-quenched state compared to that for the quenched castings (Fig. 9b). Aging of the castings of the Sn-containing alloy leads to an accelerated

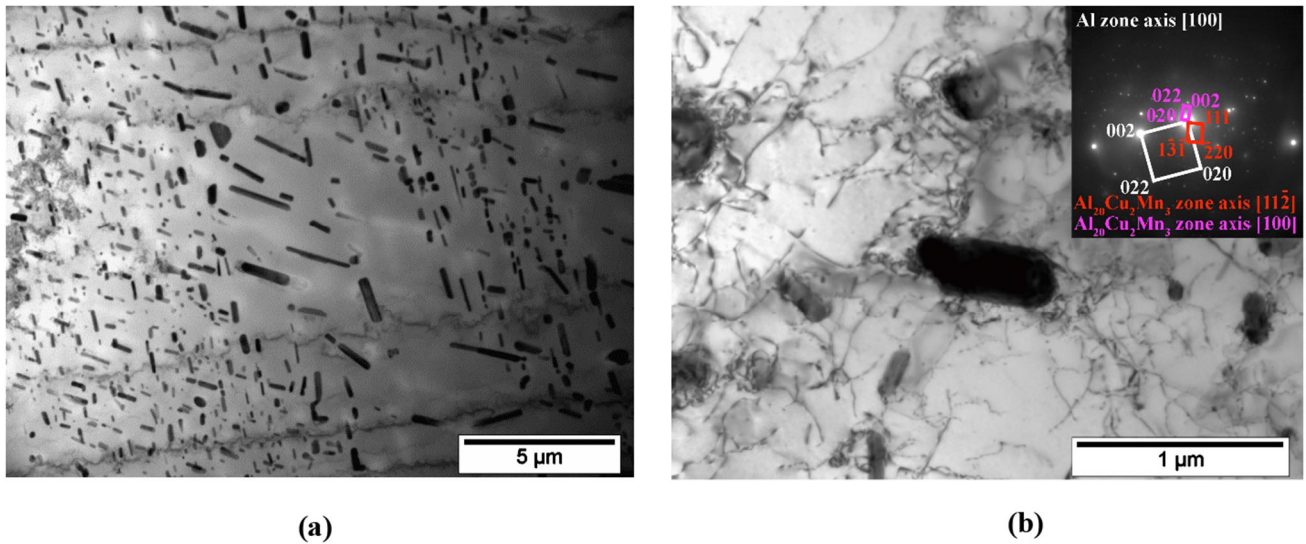


Figure 7 TEM structure of the Al4Cu1.5Mn0.1Sn alloy **a, b** after hot rolling at 400 °C followed by annealing at 510 °C for 1 h and water quenching at room temperature (~ 23 °C) and SADP taken along [100]Al zone axis.

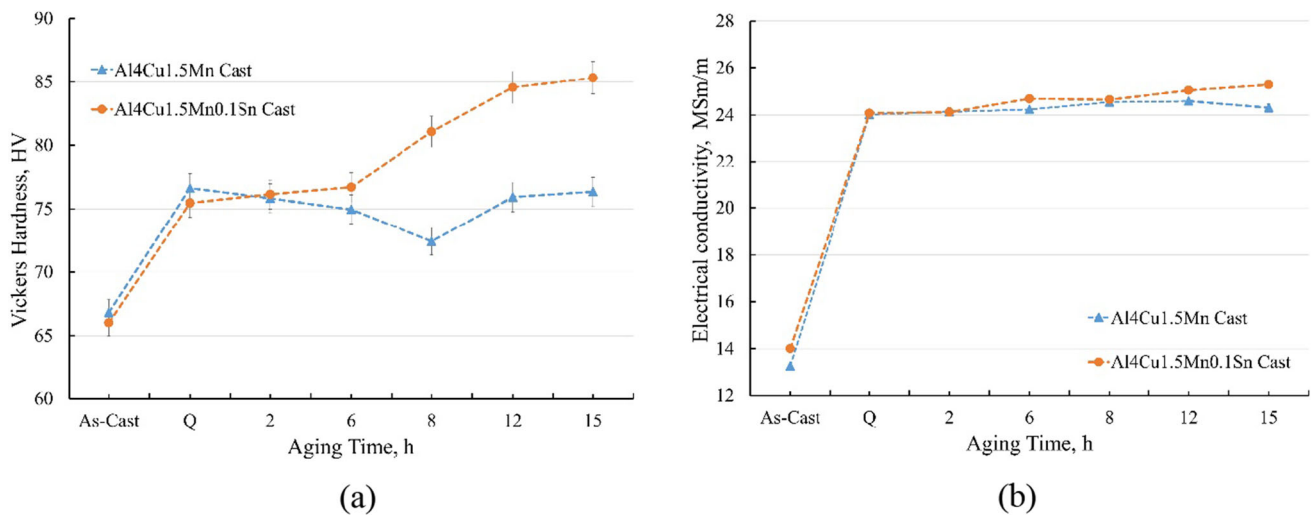


Figure 8 Dependence of **a** hardness and **b** electrical conductivity on time during aging at 175 °C of the castings annealed at 450 °C (Q-as-quenched condition).

increase in hardness which rapidly reaches the peak value of about 110–115 HV in 6–8 h and then remains almost unchanged over the rest of the experimental aging time. Thus, the hardness of the Sn-containing alloy proves to be some 43% higher than that of the Sn-free alloy. The EC of the Sn-containing alloy is also noticeably higher due to a deeper and more complete decomposition of (Al) [10, 18].

Hot rolling somewhat increases the hardness of the alloys compared to the as-cast state (Fig. 9a) and makes it close to the hardness of as-quenched castings. However, as noted above, further SS treatment leads to a drop in the hardness of both deformed

alloys to a value below that for the as-quenched castings. Further aging of the deformed Sn-containing alloy leads to an even more accelerated increase in the hardness compared to that for the castings. The slightly higher peak hardness (120 HV) is achieved in 3 h aging and then remains almost unchanged. One should note that earlier [11] we showed for the ternary Al3.5Cu0.1Sn alloy, which is characterized by the absence of manganese and slightly higher possible solubility of copper in aluminum (~ 3.2 vs. 3.5% Cu) compared to the new model Al4Cu1.5Mn0.1Sn alloy, that the hardness after similar aging is roughly the same (the peak hardness is 125 HV) for both the

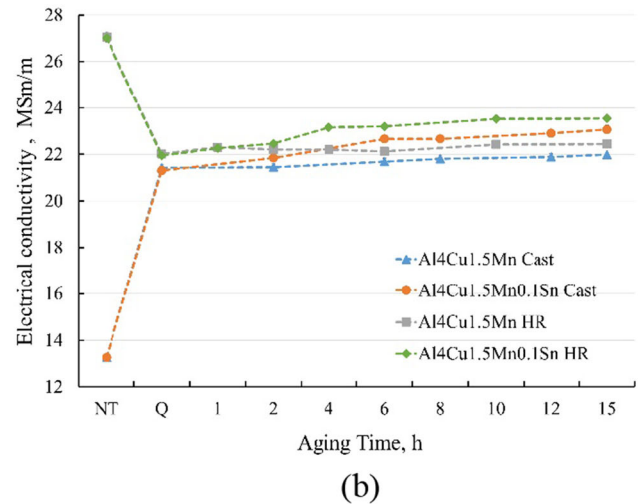
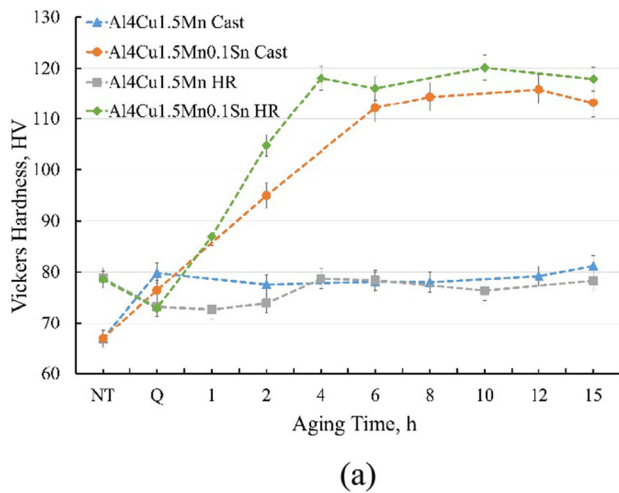


Figure 9 Dependence of **a** hardness and **b** electrical conductivity on aging time (at 175 °C) including NT [non-treated (as-cast or as-wrought)] and Q (as-quenched) conditions [the specimens were

cast and wrought samples. The EC (Fig. 9b) of the alloy in this state is higher compared with the rest states which is evidence of a superior degree of (Al) decomposition and accompanying formation of the precipitates.

Tensile tests

The mechanical properties of the considered Al4Cu1.5Mn and Al4Cu1.5Mn0.1Sn alloys in comparison with available data [3] for the industrial 2219-type alloy were also studied at uniaxial tensile tests. The mechanical properties were analyzed for the peak-aged hot-rolled sheet alloys. Typical pattern of the initially obtained engineering stress–strain curves for the alloys is presented in Fig. 10. The extracted data on the UTS, YS and relative elongation are presented as a histogram in Fig. 11 in comparison with the literary data for the industrial 2219-type alloy. The data obtained revealed that while the UTS of the Sn-containing alloy is higher than that of the Sn-free alloy by about 27% (402 MPa vs. 317 MPa), the difference in the yield strength YS is enormous: 323 MPa versus 122 MPa, i.e., by more than 2.5 times.

One should note that although the elongation of the Sn-containing alloy is smaller as compared to that of the Sn-free alloy (17.2% vs. 9.7%), it is still high enough for a ductile material. The observed decrease in elongation is associated with the natural decrease in ductility with an increase in strength and should not be considered as a negative effect of Sn trace

solid solution treated at 510 °C for 1 h followed by water quenched at room temperature (~ 23 °C)], designation HR denotes specimens subjected to hot rolling before heat treatment.

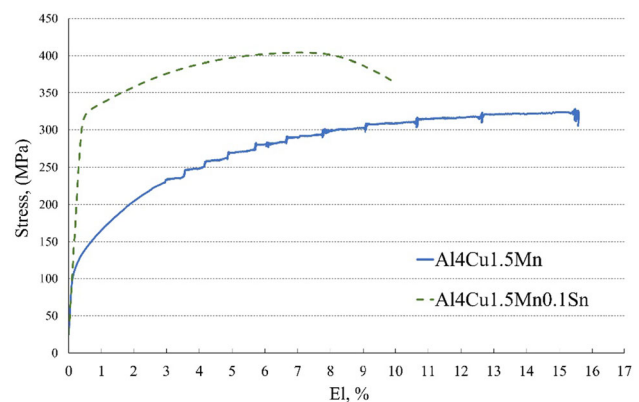


Figure 10 Characteristic tensile stress–strain diagrams of the peak-aged 2-mm hot-rolled sheets for the Al4Cu1.5Mn and Al4Cu1.5Mn0.1Sn alloys. The samples were aged at 175 °C for 3 h for the Al4Cu1.5Mn0.1Sn alloy and 10 h for the Sn-free alloy.

addition. Indeed, comparative analysis of the fracture surfaces of the alloys did not reveal any fundamental differences between them (Fig. 12). The fracture patterns for the alloys are ductile and fine dimpled, with the size of the dimples being about 2–4 μm. No traces of intergranular fracture or formation of oxide films due to local melting of tin are observed.

Discussion

TEM images of the peak-aged hot-rolled sheet alloys (Fig. 13) firmly substantiate the difference in hardness (Fig. 9a) and strength (Figs. 10 and 11) observed

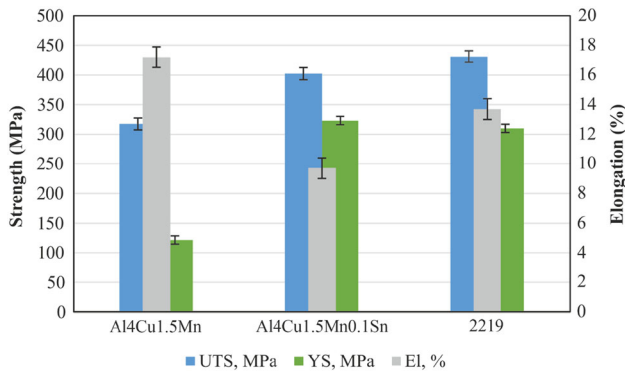
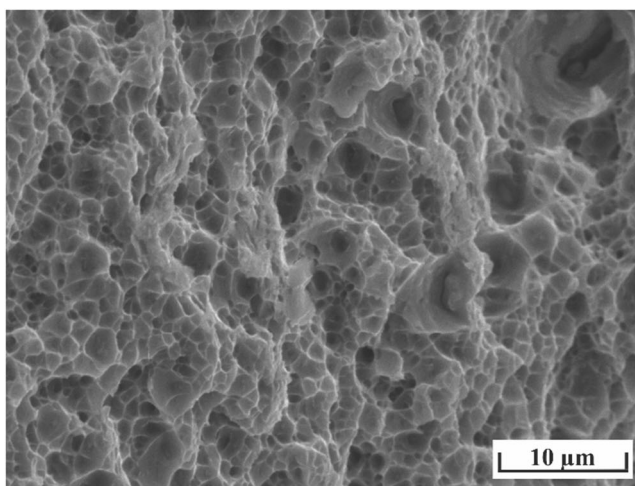


Figure 11 Mechanical properties of the peak-aged hot-rolled sheets of experimental alloy in comparison with 2219 (T6) (~ 80% reduction rate). The samples were aged at 175 °C for 3 h for the Al4Cu1.5Mn0.1Sn alloy and 10 h for the Sn-free alloy.

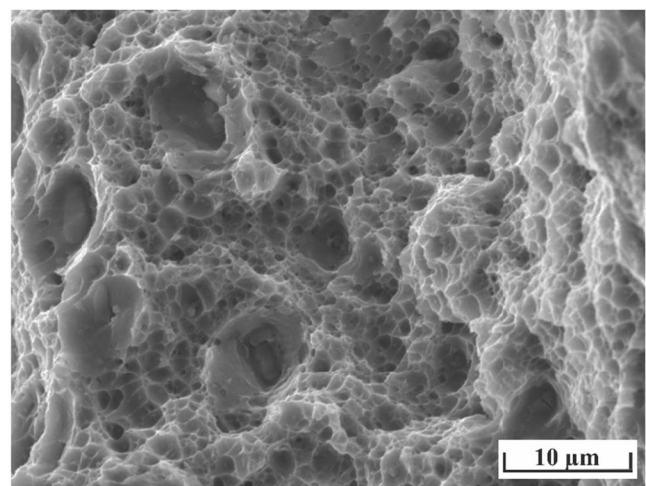
between the Al4Cu1.5Mn and Al4Cu1.5Mn0.1Sn alloys. For the Sn-free alloy (Fig. 13a and c), in the space between the relatively coarse Al₂₀Cu₂Mn₃ dispersoids, one can observe the formation of rare plate-like precipitates with an average length of 70–80 nm and a thickness of 7–9 nm. The data obtained confirm the low tendency of the base alloy to precipitation hardening. It is interesting to note while the Sn-free binary Al_{3.5}Cu alloy shows but slight tendency to precipitation strengthening at aging (the hardness increases to ~ 105 HV) [11], the Sn-free ternary Al4Cu1.5Mn alloy shows no tendency to precipitation hardening at all. In our opinion, the latter fact may be associated with the influence of the extended

(Al)/Al₂₀Cu₂Mn₃ interface which acts as an effective sink for vacancies. The influence of the extended interface for the Sn-containing alloy is negligible since the excess energy of interaction between vacancies and solute Sn trace atoms prevents the annihilation of excess vacancies during alloy quenching.

However, addition of 0.1 wt% Sn dramatically changes the precipitation structure (Fig. 13b and d). One can observe the formation of precipitates with an increased number density. According to the obtained diffraction patterns, the observed precipitates belong to the θ' phase (Fig. 13d). The linear size of the observed precipitates is at least 1.5 times less than that for the base ternary alloy. One should note that the observed structure of the Al4Cu1.5Mn0.1Sn alloy after a full cycle of thermomechanical treatment including deformation followed by solid solution treatment and aging can be characterized as the so-called hierarchical structure [42, 43]. This structure consists of two different precipitate types having about equal weight fractions but differing by dozens of times in the average characteristic size. Indeed, due to the much higher fraction of manganese (compared to the industrial alloys), one can observe the formation of a greater quantity of Al₂₀Cu₂Mn₃ phase dispersoids (~ 6.75 wt% at 510 °C according to thermodynamic calculation (Table 2)) which is about equal to that of the main strengthening θ' -phase (see Fig. 2 for the (Al) composition at 3–4 wt% Cu).



(a)



(b)

Figure 12 Fracture surfaces of the peak-aged 2 mm hot-rolled sheets after tensile test: **a** Al4Cu1.5Mn; **b** Al4Cu1.5Mn0.1Sn. SEM. The samples were aged at 175 °C for 3 h for the Al4Cu1.5Mn0.1Sn alloy and 10 h for the Sn-free alloy.

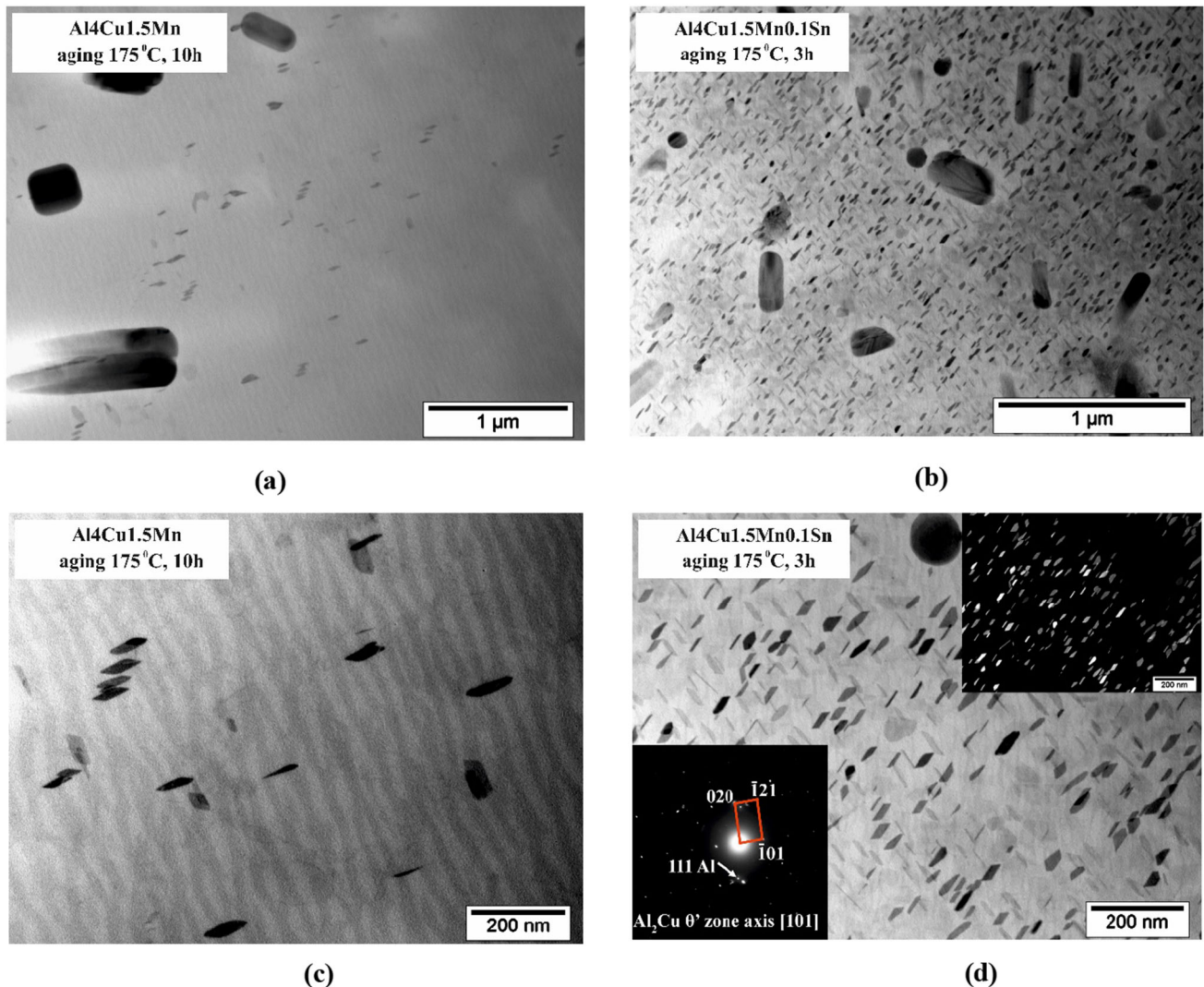


Figure 13 TEM images of the peak-aged Al₄Cu_{1.5}Mn (a, c) and Al₄Cu_{1.5}Mn_{0.1}Sn (b, d) hot-rolled sheet alloys. The samples were aged at 175 °C for 3 h for the Al₄Cu_{1.5}Mn_{0.1}Sn alloy and 10 h

for the Sn-free alloy. **d** also represents SADP taken along [101] θ' zone axis (bottom left figure) and a dark field image (top right figure).

Whereas the fine θ' -phase precipitates with an average characteristic size of tens of nanometers (Fig. 13b and d) are effective in strengthening (Fig. 9a) at temperatures up to 200–250 °C [44, 45], coarser Al₂₀Cu₂Mn₃ phase dispersoids with an average characteristic size of hundreds of nanometers (Figs. 6, 7, 13) may be effective in strengthening at higher temperatures, up to 350–400 °C [3].

The obtained difference in the YS (Fig. 10, 11) is a direct consequence of the difference in the precipitation structure of the alloys (Fig. 13). Indeed, as one can see from Fig. 9b, the EC of both cast and wrought Sn-free alloys remains virtually unchanged at aging. The latter fact suggests a very slight tendency (it

practically absent) to decomposition of the aluminum solid solution. On the contrary, at aging of the Sn-containing alloy, the EC increases markedly (Fig. 9b) as a consequence of the decomposition of the solid solution. The latter is accompanied by an increase in the number density (Fig. 13b and d) of fine precipitates determining the resultant strength properties. Thus, tin trace addition significantly improves the mechanical properties by modifying the structure of the precipitates and triggering a more complete decomposition of the aluminum solid solution [10, 18]. Both processes lead to a substantial increase in the number density of the precipitates.

It should be also noted that the UTS of the Sn-containing alloy is but slightly lower than that of the industrial 2219 alloy, while the YS is even somewhat higher at a comparable elongation. As it follows from thermodynamically calculated data (Fig. 2), the fraction of the strengthening θ' -phase in the 2219 alloy should be about 2.5 times that in the new Al4Cu1.5Mn0.1Sn alloy (3.7 vs. 9.0 wt%). In view of this difference, the about equal strength properties of these two alloys are marvelous and determined by the fact that tin trace addition significantly modifies the precipitation structure. Indeed, the average length of precipitates in 2219 alloy can be accepted 100 nm [46] which is about twice as high as that of the new Sn-containing alloy (Fig. 13d). Thus, although the fraction of the θ' -phase in the new Sn-containing alloy should be about 2.5 times less than in 2219, its much finer structure compensates this difference. In addition, it should be mentioned that unlike the new model alloy the 2219 alloy also contains a micro-addition of zirconium which also influences the precipitation structure [47, 48]. The effect of this addition on the structure and properties of the new Sn-containing alloy should be further studied in detail. Lower elongation of the Sn-containing alloy compared to that of 2219, given the roughly equal strength properties, can be accounted for by the presence of a much greater fraction of Al₂₀Cu₂Mn₃ phase dispersoids (Table 2). However, the latter fact can rather be considered as an advantage of the new alloy since an improvement of the strength properties at elevated temperatures can be expected for a greater fraction of dispersoids. Another advantage of the new alloy as compared with the industrial 2219 one is a much lower concentration of copper required to achieve the same strength properties. It should be obvious that much higher strength properties can be expected for the new Sn-containing alloy if its maximum copper concentration is comparable to that in the industrial one.

Also of interest is the effect of dynamic strain aging (DSA) observed in the form of serrated flow (rises in the flow stress followed by a drop to or even below the general stress level) in the tensile stress vs strain diagram of the base Al4Cu1.5Mn alloy (Fig. 10). These differences and such an unstable plastic deformation for different aluminum Al–Mg [49–54], Al–Zn–Mg [55], Al–Cu [56–58] alloy systems have attracted attention of researchers. The basic DSA

theory states that the appearance of serrated flow is ascribed to the competitive mechanism between pinning and unpinning effects because of the interaction between solute atoms and mobile dislocations [49, 54, 58]. During DSA the diffusion of solute atoms to mobile dislocations causes pinning, ones pile up at these obstacles and form super-dislocations [58]. Indeed, as discussed above and shown earlier [10, 18], even upon aging the aluminum solid solution of the Sn-free alloy should still be largely saturated with dissolved copper atoms. Due to the interaction between the latter ones and dislocations, one can expect the above-mentioned pinning effect. When the density of super-dislocations provides sufficient stress fields, the avalanche motion of dislocations is beginning [58]. Once they are released, a rapid stress-drop takes place until the dislocations are blocked again [57]. Thus, this mechanism explains adequately well the appearance of serrations during the tensile tests of the base Al4Cu1.5Mn aluminum alloys. However, the above-mentioned effect is missing in the Sn-containing alloy (Fig. 10). One of the origins is the formation of a much sparingly alloyed aluminum solid solution at aging, and another one is the presence of fine θ' -phase precipitates with a high number density leading to a multiple increase in the flow stress which becomes much higher than the stress caused by the interaction between dissolved atoms and dislocations.

By and large, based on the obtained data one should note that Sn trace addition in the Al–Cu–Mn-based wrought alloys is quite effective for achieving either a higher strength compared to that of the Sn-free alloy or the same strength at a far lower copper content. Moreover, the data proved that Sn trace addition does not lead to sacrifice in ductility and allows one to increase the fraction of Al₂₀Cu₂Mn₃phasedispersoids.

Conclusions

The effect of 0.1% Sn addition on the microstructure, phase composition and mechanical properties of the Al4Cu1.5Mn alloy (designed for Al₂Cu precipitates and Al₂₀Cu₂Mn₃ phase dispersoids) in the wrought state and after strengthening heat treatment was studied using computational and experimental methods. The main conclusions of the study are as follows.

- (1) Addition of 1.5 wt% Mn to the Al-4 wt% Cu alloy and high-temperature annealing (at 450–510 °C) of the ingots leads to intense formation of a large amount of Al₂₀Cu₂Mn₃ phase dispersoids the weight fraction of which (it should be ~ 7 wt% according to theoretical thermodynamic assessment) is about equal to the expected weight fraction of the main strengthening θ' -phase formed at aging.
- (2) Analysis of the microhardness and specific electrical conductivity of both cast and hot-rolled Al4Cu1.5Mn-based model alloys reveals that Sn trace addition (with a concentration of 0.1 wt%) leads to a strong increase in the precipitation hardening response compared to the Sn-free alloy. The peak hardness achieved after 175 °C aging of the wrought model Al4Cu1.5Mn0.1Sn alloy is ~ 120 HV which is about 43% higher than that of the Sn-free Al4Cu1.5Mn alloy.
- (3) TEM images of the peak-aged hot-rolled sheet alloys firmly substantiate the observed difference in the hardness between the model alloys. Rare plate-like precipitates with an average length of 70–80 nm form in the Sn-free alloy. However, addition of 0.1 wt% Sn dramatically changed the precipitation structure. Much finer precipitates are observed (with an average length of 55–60 nm) having an incomparably higher number density.
- (4) The mechanical properties analyzed at tensile tests of the peak-aged hot-rolled sheet Al4Cu1.5Mn and Al4Cu1.5Mn0.1Sn alloys revealed that tin trace addition allows one to increase the UTS of the alloy by about 27% (402 MPa vs. 317 MPa), while the difference in the yield strength YS is enormous: 323 MPa versus 122 MPa, i.e., by more than 2.5 times. At the same time, the Al4Cu1.5Mn0.1Sn alloy still has a high ductility (~ 10%). The obtained difference in the strength properties is a direct consequence of the difference in the precipitation structure of the alloys.
- (5) The obtained mechanical properties of the model Al4Cu1.5Mn0.1Sn alloy are very close to those of the industrial 2219-type alloy containing one and a half times more copper. However, the new alloy contains a superior fraction of Al₂₀Cu₂Mn₃ phase dispersoids the

influence of which on the mechanical properties should be further studied in detail.

Acknowledgements

The study was carried out with the financial support of the grant of the Russian Science Foundation (Project No 20-79-10373, link to information about the project: <https://rscf.ru/en/project/20-79-10373/>).

Data availability

The raw/processed data required to reproduce these findings cannot be shared at this time due to technical or time limitations.

Declarations

Conflict of interest The authors declare that they have no known competing financial interests or personal relationships that could have appeared to influence the work reported in this paper.

Ethical approval Not applicable.

References

- [1] Dar SM, Liao H (2019) Creep behavior of heat resistant Al–Cu–Mn alloys strengthened by fine (θ') and coarse (Al₂₀Cu₂Mn₃) second phase particles. *Mater Sci Eng A* 763:138062. <https://doi.org/10.1016/j.msea.2019.138062>
- [2] Sun T, Geng J, Bian Z, Wu Y, Wang M, Chen D, Ma N, Wang H (2022) Enhanced thermal stability and mechanical properties of high-temperature resistant Al–Cu alloy with Zr and Mn micro-alloying. *T Nonferr Metal Soc* 32:64–78. [https://doi.org/10.1016/S1003-6326\(21\)65778-3](https://doi.org/10.1016/S1003-6326(21)65778-3)
- [3] Belov NA, Akopyan TK, Shurkin PK, Korotkova NO (2021) Comparative analysis of structure evolution and thermal stability of commercial AA2219 and model Al–2 wt%Mn–2 wt%Cu cold rolled alloys. *J Alloys Compd* 864:158823. <https://doi.org/10.1016/j.jallcom.2021.158823>
- [4] Silcock JM, Heal TJ, Hardy HK (1953–1954) Structural ageing characteristics of aluminum–copper alloys. *J Inst Met* 82:239–248
- [5] Biswas A, Siegel DJ, Wolverson C, Seidman DN (2011) Precipitates in Al–Cu alloys revisited: atom-probe tomographic experiments and first-principles calculations of compositional evolution and interfacial segregation. *Acta*

- Mater 59:6187–6204. <https://doi.org/10.1016/j.actamat.2011.06.036>
- [6] Bourgeois L, Dwyer C, Weyland M, Nie J, Muddle BC (2011) Structure and energetics of the coherent interface between the θ' precipitate phase and aluminium in Al–Cu. *Acta Mater* 59:7043–7050. <https://doi.org/10.1016/j.actamat.2011.07.059>
- [7] Shen Z, Ding Q, Liu C, Wang J, Tian H, Li J, Zhang Z (2017) Atomic-scale mechanism of the $\theta'' \rightarrow \theta'$ phase transformation in Al–Cu alloys. *J Mater Sci Technol* 33:1159–1164. <https://doi.org/10.1016/j.jmst.2016.08.031>
- [8] Zuiko I, Kaibyshev R (2018) Aging behavior of an Al–Cu–Mg alloy. *J Alloys Compd* 759:108–119. <https://doi.org/10.1016/j.jallcom.2018.05.053>
- [9] Akopyan TK, Belov NA, Letyagin NV (2019) Effect of Trace Addition of Sn on the Precipitation Hardening in Al–Si–Cu Eutectic Alloy. *JOM* 71:1768–1775. <https://doi.org/10.1007/s11837-019-03422-x>
- [10] Akopyan TK, Belov NA, Lukyanchuk AA, Letyagin NV, Milovich FO, Fortuna AS (2022) Characterization of structure and hardness at aging of the A319 type aluminum alloy with Sn trace addition. *J Alloys Compd* 921:166109. <https://doi.org/10.1016/j.jallcom.2022.166109>
- [11] Akopyan TK, Shurkin PK, Letyagin NV, Milovich FO, Fortuna AS, Koshmin AN (2021) Structure and precipitation hardening response in a cast and wrought Al–Cu–Sn alloy. *Mater Lett* 300:130090. <https://doi.org/10.1016/j.matlet.2021.130090>
- [12] Bourgeois L, Dwyer C, Weyland M, Nie J-F, Muddle BC (2012) The magic thicknesses of θ' precipitates in Sn-microalloyed Al–Cu. *Acta Mater* 60:633–644. <https://doi.org/10.1016/j.actamat.2011.10.015>
- [13] Dai S, Bian Z, Wu W, Tao J, Cai L, Wang M, Xia C, Wang H (2020) The role of Sn element on the deformation mechanism and precipitation behavior of the Al–Cu–Mg alloy. *Mater Sci Eng A* 792:139838. <https://doi.org/10.1016/j.msea.2020.139838>
- [14] Zhang X, Liu M, Wang J et al (2022) Combined effect of Sn addition and pre-ageing on natural secondary and artificial ageing of Al–Mg–Si alloys. *J Mater Sci* 57:2149–2162. <https://doi.org/10.1007/s10853-021-06654-y>
- [15] Zhang Y, Zhang Z, Medhekar NV, Bourgeois L (2017) Vacancy-tuned precipitation pathways in Al–1.7Cu–0.025In–0.025Sb (at.%) alloy. *Acta Mater* 141:341–351. <https://doi.org/10.1016/j.actamat.2017.09.025>
- [16] Shurkin PK, Akopyan TK, Letyagin NV (2021) Effect of indium microaddition on the structure and strengthening of binary Al–Cu alloys. *Phys Met Metallogr* 122:807–813. <https://doi.org/10.1134/S0031918X21080159>
- [17] Berezina AL, Monastyrskaya TO, Molebny OA, Fikssen VN, Rud AD, Kotko AV (2020) Effect of microalloying with transition and post-transition metals on the aging of precipitation-hardened Al–Cu alloys. *Appl Nanosci* 10:4773–4780. <https://doi.org/10.1007/s13204-020-01322-0>
- [18] Akopyan TK, Belov NA, Letyagin NV, Milovich FO, Lukyanchuk AA, Fortuna AS (2022) Influence of indium trace addition on the microstructure and precipitation hardening response in Al–Si–Cu casting aluminum alloy. *Mater Sci Eng A* 831:142329. <https://doi.org/10.1016/j.msea.2021.142329>
- [19] Hu Y, Wang G, Ye M, Wang S, Wang L, Rong Y (2018) A precipitation hardening model for Al–Cu–Cd alloys. *Mater Des* 151:123–132. <https://doi.org/10.1016/j.matdes.2018.04.057>
- [20] Liu X, Wang G, Hu Y, Ji Y, Rong Y, Hu Y, Chen L-Q (2021) Multi-scale simulation of Al–Cu–Cd alloy for yield strength prediction of large components in quenching aging process. *Mater Sci Eng A* 814:141223. <https://doi.org/10.1016/j.msea.2021.141223>
- [21] Staab TEM, Lotter F, Mühle U et al (2021) The decomposition process in high-purity Al–1.7 at.% Cu alloys with trace elements: preservation of quenched-in vacancies by In, Sn and Pb influencing the θ' formation. *J Mater Sci* 56:8717–8731. <https://doi.org/10.1007/s10853-020-05742-9>
- [22] Robson JD, Engler O, Sigli C, Deschamps A, Poole WJ (2020) Advances in microstructural understanding of wrought aluminum alloys. *Metall Mater Trans A* 51:4377–4389. <https://doi.org/10.1007/s11661-020-05908-9>
- [23] Gazizov M, Kaibyshev R (2017) Precipitation structure and strengthening mechanisms in an Al–Cu–Mg–Ag alloy. *Mater Sci Eng A* 702:29–40. <https://doi.org/10.1016/j.msea.2017.06.110>
- [24] Rosalie JM, Bourgeois L (2012) Silver segregation to θ' (Al₂Cu)–Al interfaces in Al–Cu–Ag alloys. *Acta Mater* 60:6033–6041. <https://doi.org/10.1016/j.actamat.2012.07.039>
- [25] Kang SJ, Kim Y-W, Kim M, Zuo J-M (2014) Determination of interfacial atomic structure, misfits and energetics of X phase in Al–Cu–Mg–Ag alloy. *Acta Mater* 81:501–511. <https://doi.org/10.1016/j.actamat.2014.07.074>
- [26] Bai S, Liu Z, Zhou X, Xia P, Zeng S (2014) Mg-controlled formation of Mg–Ag co-clusters in initial aged Al–Cu–Mg–Ag alloys. *J Alloys Compd* 602:193–198. <https://doi.org/10.1016/j.jallcom.2014.03.008>
- [27] Chen Y, Zhang Z, Chen Z, Tsalanidis A, Weyland M, Findlay S, Allen LJ, Lie J, Medhekar NV, Bourgeois L (2017) The enhanced theta-prime (θ') precipitation in an Al–Cu alloy with trace Au additions. *Acta Mater* 125:340–350. <https://doi.org/10.1016/j.actamat.2016.12.012>

- [28] Klobes B, Balarisi O, Liu M, Staab TEM, Maier K (2010) The effect of microalloying additions of Au on the natural ageing of Al–Cu. *Acta Mater* 58:6379–6384. <https://doi.org/10.1016/j.actamat.2010.07.059>
- [29] Lotter F, Petschke D, Geuser F, Elsayed M, SEXTL G, Staab TEM (2019) In situ natural ageing of Al–Cu–(Mg) alloys: the effect of In and Sn on the very early stages of decomposition. *Scr Mater* 168:104–107. <https://doi.org/10.1016/j.scriptamat.2019.04.031>
- [30] Kimura H, Kimura A, Hasiguti R (1962) A resistometric study on the role of quenched-in vacancies in ageing of Al–Cu alloys. *Acta Metall* 10:607–619. [https://doi.org/10.1016/0001-6160\(62\)90050-0](https://doi.org/10.1016/0001-6160(62)90050-0)
- [31] Wolverton C (2007) Solute-vacancy binding in aluminum. *Acta Mater* 55:5867–5872. <https://doi.org/10.1016/j.actamat.2007.06.039>
- [32] Ohkubo H, Nagai Y, Inoue K, Tang Z, Hasegawa M (2004) Vacancy-solute binding energies in aluminum by positron annihilation. *Mater Sci Forum* 445–446:165–167. <https://doi.org/10.4028/www.scientific.net/MSF.445-446.165>
- [33] Wang RH, Wen Y, Chen BA (2021) Sn microalloying Al–Cu alloys with enhanced fracture toughness. *Mater Sci Eng A* 814:141243. <https://doi.org/10.1016/j.msea.2021.141243>
- [34] Information on <http://www.thermocalc.com>.
- [35] Glazoff MV, Khvan AV, Zolotarevsky VS, Belov NA, Dinsdale AT (2018) Casting aluminum alloys: their physical and mechanical metallurgy, 2nd edn. Butterworth-Heinemann, Oxford
- [36] McAllister AJ, Kahan D (1983) The Al–Sn (aluminum-tin) system. *Bull Alloy Phase Diagr* 4:410–414. <https://doi.org/10.1007/BF02868095>
- [37] Mondolfo LF (1976) Aluminum alloys: structure and properties, 1st edn. Butterworth-Heinemann, London
- [38] Feng ZQ, Yang YQ, Huang B, Li MH, Chen YX, Ru JG (2014) Crystal substructures of the rotation-twinned T (Al₂₀Cu₂Mn₃) phase in 2024 aluminum alloy. *J Alloys Compd* 583:445–451. <https://doi.org/10.1016/j.jallcom.2013.08.200>
- [39] Polmear IJ (2006) Light alloys: from traditional alloys to nanocrystals, 4th edn. Butterworth-Heinemann, Oxford
- [40] Belov NA, Korotkova NO, Akopyan TK, Tsydenov KA (2019) Simultaneous increase of electrical conductivity and hardness of Al–1.5 wt% Mn alloy by addition of 1.5 wt% Cu and 0.5 wt% Zr. *Metals* 9:1246–1245. <https://doi.org/10.3390/met9121246>
- [41] Belov NA, Akopyan TK, Korotkova NO, Shurkin PK, Timofeev VN, Raznitsyn OA, Sviridova TA (2022) Structure and heat resistance of high strength Al–3.3% Cu–2.5% Mn–0.5% Zr (wt%) conductive wire alloy manufactured by electromagnetic casting. *J Alloys Compd* 891:161948. <https://doi.org/10.1016/j.jallcom.2021.161948>
- [42] Wu SH, Xue H, Yang C, Kuang J, Zhang P, Zhang JY, Li YJ, Roven HJ, Liu G, Sun J (2021) Hierarchical structure in Al–Cu alloys to promote strength/ductility synergy. *Scr Mater* 202:113996. <https://doi.org/10.1016/j.scriptamat.2021.113996>
- [43] Yang C, Cao L, Gao Y, Cheng P, Zhang P, Kuang J, Zhang J, Liu G, Sun J (2020) Nanostructural Sc-based hierarchy to improve the creep resistance of Al–Cu alloys. *Mater Des* 186:108309. <https://doi.org/10.1016/j.matdes.2019.108309>
- [44] Roy S, Allard LF, Rodriguez A, Porter WD, Shyam A (2017) Comparative evaluation of cast aluminum alloys for automotive cylinder heads: part II—mechanical and thermal properties. *Metall Mater Trans A* 48:2543–2562. <https://doi.org/10.1007/s11661-017-3986-0>
- [45] Milligan BK, Roy S, Hawkins CS, Allard LF, Shyam A (2020) Impact of microstructural stability on the creep behavior of cast Al–Cu alloys. *Mater Sci Eng A* 772:138697. <https://doi.org/10.1016/j.msea.2019.138697>
- [46] Xu D, Zhu C, Xu C, Chen K (2021) Microstructures and tensile fracture behavior of 2219 wrought Al–Cu alloys with different impurity of Fe. *Metals* 11:174. <https://doi.org/10.3390/met11010174>
- [47] Mondol S, Kashyap S, Kumar S, Chattopadhyay K (2018) Improvement of high temperature strength of 2219 alloy by Sc and Zr addition through a novel three-stage heat treatment route. *Mater Sci Eng A* 732:157–166. <https://doi.org/10.1016/j.msea.2018.07.003>
- [48] Jiang L, Rouxel B, Langan T, Dorin T (2021) Coupled segregation mechanisms of Sc, Zr and Mn at θ' interfaces enhances the strength and thermal stability of Al–Cu alloys. *Acta Mater* 206:116634. <https://doi.org/10.1016/j.actamat.2021.116634>
- [49] Bakare F, Schieren L, Rouxel B, Jiang L, Langan T, Kupke A, Weiss M, Dorin T (2021) The impact of L12 dispersoids and strain rate on the Portevin–Le–Chatelier effect and mechanical properties of Al–Mg alloys. *Mater Sci Eng A* 811:141040. <https://doi.org/10.1016/j.msea.2021.141040>
- [50] He P, Webster RF, Yakubov V, Kong H, Yang Q, Huang S, Ferry M, Kruzic JJ, Li X (2021) Fatigue and dynamic aging behavior of a high strength Al–5024 alloy fabricated by laser powder bed fusion additive manufacturing. *Acta Mater* 220:117312. <https://doi.org/10.1016/j.actamat.2021.117312>
- [51] Nie X, Zhang H, Zhu H, Hu Z, Qi Y, Zeng X (2019) On the role of Zr content into Portevin–Le–Chatelier (PLC) effect of selective laser melted high strength Al–Cu–Mg–Mn alloy. *Mater Lett* 248:5–7. <https://doi.org/10.1016/j.matlet.2019.03.112>
- [52] Zhemchuzhnikova D, Lebyodkin M, Yuzbekova D, Lebedkina T, Mogucheveva A, Kaibyshev R (2018) Interrelation

- between the Portevin–Le–Chatelier effect and necking in AlMg alloys. *Int J Plast* 110:95–109. <https://doi.org/10.1016/j.ijplas.2018.06.012>
- [53] Zhemchuzhnikova DA, Lebyodkin MA, Lebedkina TA, Kaibyshev RO (2015) Unusual behavior of the Portevin–Le–Chatelier effect in an AlMg alloy containing precipitates. *Mater Sci Eng A* 639:37–41. <https://doi.org/10.1016/j.msea.2015.04.094>
- [54] Xu J, Holmedal B, Hopperstad OS, M´anik T, Marthinsen K (2022) Dynamic strain ageing in an AlMg alloy at different strain rates and temperatures: experiments and constitutive modelling. *Int J Plast* 151:103215. <https://doi.org/10.1016/j.ijplas.2022.103215>
- [55] Cai Y, Yang S, Fu S, Zhang D, Zhang Q (2017) Investigation of Portevin–Le–Chatelier band strain and elastic shrinkage in Al-based alloys associated with Mg contents. *J Mater Sci Technol* 33:580–586. <https://doi.org/10.1016/j.jmst.2016.05.012>
- [56] Krasnikov VS, Mayer AE, Pogorelko VV, Gazizov MR (2021) Influence of θ' phase cutting on precipitate hardening of Al–Cu alloy during prolonged plastic deformation: molecular dynamics and continuum modeling. *Model Appl Sci* 11:4906. <https://doi.org/10.3390/app11114906>
- [57] Sun L, Zhang Q, Huifeng J (2007) Effect of solute concentration on Portevin–Le–Chatelier effect in Al–Cu alloys. *Front Mater Sci China* 1(2):173–176. <https://doi.org/10.1007/s11706-007-0031-z>
- [58] Peng K, Chen W, Zhangw H, Qian K-W (1997) Features of dynamic strain aging in high strength Al–Zn–Mg–Cu alloy. *Mater Sci Eng A* 234–236:138–141. [https://doi.org/10.1016/S0921-5093\(97\)00171-8](https://doi.org/10.1016/S0921-5093(97)00171-8)

Publisher’s Note Springer Nature remains neutral with regard to jurisdictional claims in published maps and institutional affiliations.

Springer Nature or its licensor (e.g. a society or other partner) holds exclusive rights to this article under a publishing agreement with the author(s) or other rightsholder(s); author self-archiving of the accepted manuscript version of this article is solely governed by the terms of such publishing agreement and applicable law.